23 Reproducible Sample Preparation and Spectrum Acquisition Techniques for Metabolic Profiling of Human Tissues by Proton High-Resolution Magic Angle Spinning Nuclear Magnetic Resonance

Martial Piotto, François-Marie Moussallieh, Alessio Imperiale, Malika A. Benahmed, Julien Detour, Jean-Pierre Bellocq, Izzie J. Namer, and Karim Elbayed

High-resolution magic angle spinning (HR-MAS) is a nuclear magnetic resonance (NMR) technique (1–3) that enables the characterization of metabolic phenotypes of intact cells, tissues, and organs under normal and pathological conditions. As with NMR in general, HR-MAS can be applied to a variety of NMR-active nuclei. However, this chapter is exclusively concerned with the proton-based (^{1}H) variant, which is the most commonly used HR-MAS method. Therefore, in the remainder of this chapter, "NMR" and "HR-MAS" are synonymous with "^{1}H NMR" and "^{1}H HR-MAS." A brief introduction of NMR basics and an example of ^{31}P HR-MAS NMR spectroscopy are presented in Chapter 22. HR-MAS can be used to assess cellular metabolic networks that are directly related to specific genetic information and to the regulation of specific gene transcripts. The basic principle of HR-MAS is to spin samples at a 54.7-degree angle ("magic angle") with respect to the main magnetic field, B_0, to remove most of the line broadening created by magnetic susceptibility gradients in heterogeneous systems such as biopsy specimens (3–8). Magic-angle spinning results in a dramatic sharpening of the NMR signals of the metabolites contained in a biopsy sample. The first applications of HR-MAS to biological tissues were published in 1996 by Cheng et al. (9). In this seminal publication, data obtained on malignant lymph nodes and on tissue samples from different brain regions in a case of Pick's disease were presented. Since then, the technique has been applied to study various pathologies in brain (10–15), breast (16–21), prostate (22–25), kidney (26–28), cervix (29,30), esophagus (31), and colon (32–34). Several reviews describing HR-MAS studies of different human malignancies have appeared in the literature more recently (35–37). However, most of the studies reported until now have been performed on a small number of biopsy samples and only in academic research laboratories (as opposed to a hospital environment). Certain procedures used in these studies can differ substantially from laboratory to laboratory, making it difficult to compare results. There

is a need for establishing a well-defined protocol covering all aspects of a large-scale metabolic study of biopsy samples. The same fundamental problem had to be solved previously for metabolic studies of urine, plasma, serum, and tissue extracts, and standard protocols eventually were adopted for some of these analyses (38,39) (biofluid NMR methods are described in Chapters 11 through 17). Regarding the study of human biopsy specimens, the situation has been more confusing than for biofluids because only one article by Beckonert et al. (40) has detailed a protocol for the study of biopsy samples by HR-MAS. This article is extremely valuable and describes the essential steps that have to be followed for a successful study. However, the authors' protocol was not embedded in the context of a medical environment where tissue samples have to be analyzed within the regular flow of routine analysis taking place daily in a hospital. Notwithstanding, the HR-MAS NMR spectroscopic protocols employed by groups working on human samples have begun to converge in recent years, and the rough contours of a consensus are emerging.

This chapter is a first attempt to standardize formally the protocols being used in this field and is part of the CARMeN (*Cancer Résonance Magnétique Nucléaire*) project carried out at the Strasbourg University Hospitals. This chapter describes the current stage of the development of a general protocol for HR-MAS NMR spectroscopy of human biopsy specimens, optimized for use in a hospital environment. This work is based on the results of more than 5 years of practical progress toward establishing a common, clinically relevant approach. The techniques described in the sections of this chapter are widely used today in laboratories analyzing human biopsy samples by HR-MAS NMR spectroscopy, but alternative approaches are also pointed out. The different steps involved in these experimental protocols are explained in detail, and the underlying rationales are presented, followed by some practical application examples in sections 7 and 8. Reliable metabolic profiling of human biopsy samples can be achieved only if numerous conditions are met in the protocol used for analysis. To illustrate the subject of this study, we present in Figure 23.1 a representative HR-MAS one-dimensional (1D) CPMG (41) ^{1}H NMR spectrum obtained from an oligodendroglioma biopsy sample, which is a grade II/III brain tumor (42). Many metabolites are easily identified in this spectrum, such as creatine (Cr) and choline (Cho). Characteristic brain metabolites such as *N*-acetyl aspartate (NAA) and γ-aminobutyric acid (GABA) are also visible.

1. Sample Collection and Storage

Proper sample collection is one of the most critical aspects of successful HR-MAS analysis of human biopsy specimens. In contrast to metabolic studies performed on body fluids – notably urine, plasma, serum, and semen – where sample collection is relatively straightforward, taking a tissue sample from a patient is an invasive process. HR-MAS studies of human tissue, in contrast to studies performed on animal models, need to be carefully integrated into a standard medical procedure. Typically, tissue samples are collected by a surgeon during an operation either as a small biopsy specimen or as a large part of an organ during an exeresis (ablation

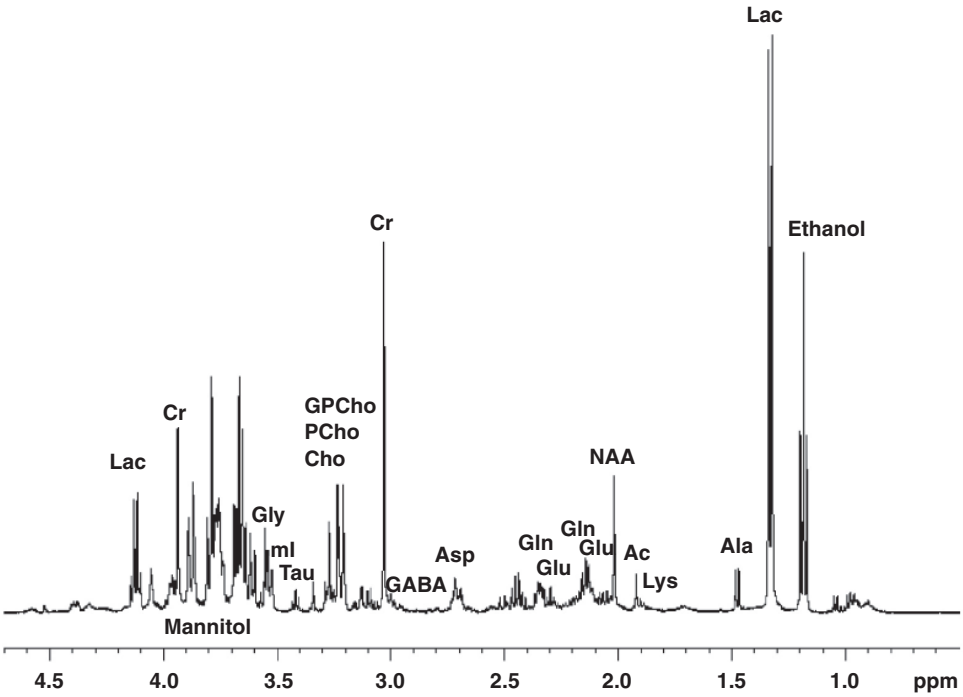

Figure 23.1. 1D ^{1}H HR-MAS CPMG spectrum of a human oligodendroglioma biopsy sample at 500 MHz. Characteristic metabolites are annotated. Experimental conditions: temperature 277 K, spinning speed 3.5 kHz, weight of biopsy specimen 15 mg, experiment time 10 minutes. All spectra presented in this chapter were acquired on an 11.7 T AVANCE III system (spectrometer hardware and software from Bruker Biospin, Rheinstetten, Germany).

of the organ). In the first case, the amount of tissue sample is small (a few milligrams), whereas in the second case, entire organs can be removed. In a medical setup, these tissue samples are used primarily for histopathological analysis and for biomolecular analysis. Histopathological analysis consists of studying the detailed morphological features of a tissue under a microscope using appropriate staining agents and is currently the gold standard used to evaluate tissue characteristics, providing information pertaining to the nature of the tissue (e.g., the grade of a tumor). Histopathological diagnosis plays a fundamental role in defining a patient's prognosis, treatment, and management. After surgical resection, the tissue specimens are immediately sent to the histopathology department for sampling and diagnostic purposes. At this point, a histopathologist selects the samples that are needed for histopathological diagnosis, routine biomolecular analysis, and immunochemical (IHC) and in situ hybridization (ISH) analysis with a morphological background. Samples selected for metabolic studies and future biomolecular analysis are snap-frozen and stored in a -80°C deep freezer located in the biobank of the hospital. All relevant data regarding the sample and the patient are also carefully documented for future use. At the present time, the most practical way of conducting an HR-MAS analysis of human tissue samples is to use samples available from the biobank of

a hospital. In cases where the delay between sample collection and sample freezing needs to be kept very short (less than 5 minutes) to obtain relevant metabolic information (i.e., brain tissues), snap-freezing may be performed immediately in the operating room. For animal studies, working with tissue samples is less problematic because animals can be sacrificed and samples can be collected immediately. These considerations demonstrate that quality and reproducibility of human biopsy samples depend significantly on the surgeon and on the nature of the surgical operation. One of the main parameters to control is the duration of ischemia (i.e., the amount of time during which tissue is left without blood perfusion). This time is critical because both the nature and the quantity of the metabolites detected by HR-MAS are strongly affected by the duration of ischemia. One effect of ischemia is that the amount of lactate increases significantly as a result of anaerobic glycolysis induced by hypoxia. Most tissue samples analyzed by HR-MAS show a large lactate peak. The duration of ischemia is also important for tissues used in certain histopathological analyses. However, ischemia has less influence on cellular structures than it has on metabolic profiles. To determine the total duration of tissue ischemia, two different phases of the surgical operation process need to be examined. The first phase is the removal of the tissue. To prevent excessive bleeding of the patient, the surgeon first clamps the veins and the arteries surrounding the tissue to be excised. This is a required step for many organs (e.g., colon, lung, ovary, kidney) but not for the brain. The associated duration of ischemia depends on the surgeon, the organ operated, and the complexity of the operation. The second phase during which ischemia occurs is after tissue removal. In routine surgery, removed tissue is often left standing in a recipient on the operating table at room temperature before storage in nitrogen. Although the duration of the first phase is strictly defined by the surgical process, the second ischemic delay can be reduced dramatically without adverse effects on the patient's health. While the sample is exposed to room temperature, enzymatic and chemical reactions are active and lead to biochemical degradation processes. Sample degradation is more rapid in some organs than in others. In particular, some metabolites of brain tissue are known to degrade at a faster rate than in many other tissues. For example, in brain specimens, *N*-acetyl aspartate (NAA) is rapidly transformed to acetate and aspartate at room temperature (43,44).

An example of a degradation study of a healthy lung biopsy specimen at 24°C is shown in Figure 23.2. The purpose of this experiment was to simulate the combined effects of 1) the second ischemic delay, and 2) the duration of sample rotation during HR-MAS on the metabolic profile of the lung. The first spectrum was recorded at 4°C with a fresh sample at $t = 0$. Between each successive experiment, the sample was taken out of the magnet and left standing at room temperature. These spectra show that the metabolic profile of the biopsy sample changed over time. In particular, the signal intensities for glucose (4.65 ppm), phosphorylcholine (3.22 ppm), choline (3.20 ppm), acetate (1.90 ppm), and alanine (1.48 ppm) increased significantly, whereas ascorbic acid (4.53 ppm) decreased. The fact that the apparent concentrations of most metabolites increase with natural sample degradation and with repeated cycles of sample spinning has been noted by several authors (45). This effect is most likely due to progressive degradation of tissue structure.

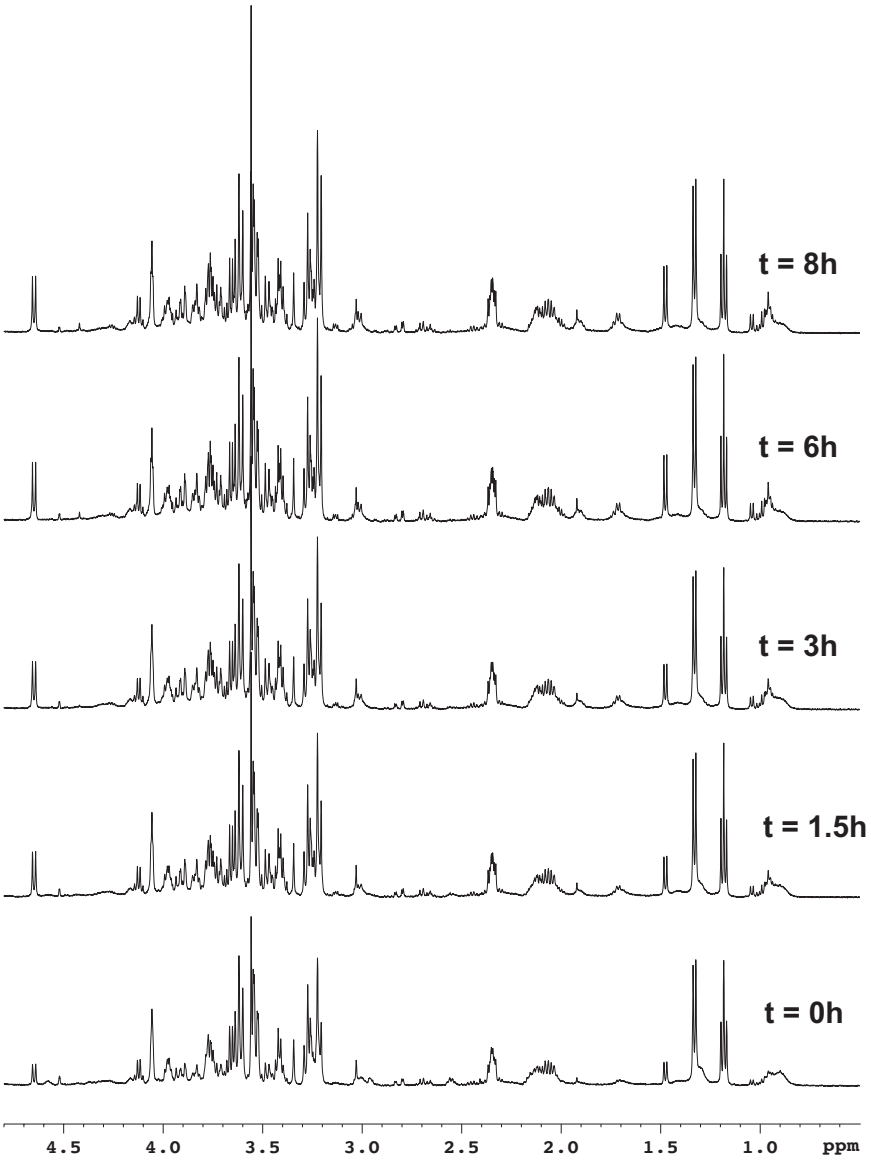

Figure 23.2. Degradation study of a control lung biopsy specimen performed at 24°C to simulate the second time of ischemia. Spectra were recorded at time 0, 1.5, 3, 6, and 8 hours. Between each experiment, the sample was taken out of the NMR instrument and kept at room temperature.

In intact tissue, macromolecules such as enzymes and other relatively immobile and semisolid structures bind a certain amount of small molecules, notably polar metabolites. Because these molecules are much less mobile in a bound state than they are in solution (tissue water), they generate only very broad NMR signals that are virtually undetectable by common NMR methods, as are the macromolecule signals themselves. These signals at most may deform the spectrum baseline but do not permit detailed analysis. As tissue structure decomposes, these macromolecules

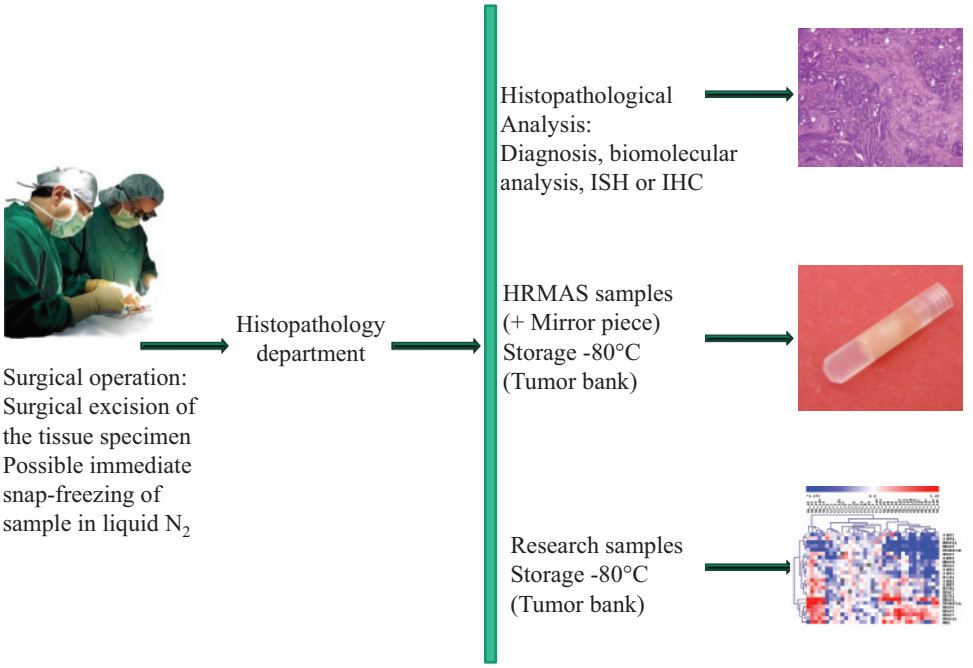

Figure 23.3. Optimized procedure for the collection of human tissues in a hospital.

and other structures with reduced molecular mobility release bound metabolites into intracellular and extracellular water. Once dissolved, these metabolites are highly mobile and become NMR-visible, increasing the intensities of the metabolite peaks in question. Consequently, the further tissue degradation progresses, the more metabolite signals increase until no more molecules are released into solution.

To guarantee tissue sample integrity as much as possible and to reduce the duration of ischemia to a minimum, we have established the following protocol (Figure 23.3). For each type of surgery, a reference person present during the surgical operation collects the surgical specimen and transfers it rapidly to the histopathology department, where a pathologist subdivides it to generate individual specimens for

1) routine histopathological analysis, which may be complemented with additional analyses, for example, biomolecular analysis, in situ hybridization (ISH), and immunohistochemistry (IHC) performed on tissues fixed with formol and embedded in paraffin;
2) further analyses based on frozen samples;
3) routine HR-MAS analysis;
4) additional analyses for research purposes.

For the HR-MAS study, two individual specimens are collected: one for the metabolic analysis itself and the other (the mirror sample) for a matched histological analysis. After this selection, the two samples for the HR-MAS study and the

research samples are stored in a −80°C deep freezer. With this procedure, the tissue sample is continuously kept at low temperature after excision in the operating room. This procedure guarantees a high degree of sample integrity, which is essential not only for HR-MAS metabolic analysis but also for biomolecular analysis. At −80°C, samples can be stored for several years with minimum alteration (46). A variant of the above-described procedure consists of selecting the final, individual specimens directly in the operating room, snap-freezing them in liquid nitrogen, and keeping them at −80°C until analysis.

Because it is known that repeated cycles of sample freezing and thawing alter the structure of tissues (47–49), it is recommended to minimize the number of cycles (typically one or two) before HR-MAS analysis. The most common sources of contamination giving rise to signals detectable by NMR in tissue samples are 1) ethanol (peaks at 1.18 ppm and 3.65 ppm), which is used for sterilization of surgical instruments, and 2) optimum cutting temperature (OCT) cryoprotective embedding medium that contains soluble glycols and resins. OCT medium might be detectable in samples that were previously used, at least in part, for a histopathological study. The OCT signal is easily identified in 1D ^{1}H spectra because it gives rise to a large singlet at 3.70 ppm. Samples containing a large amount of either of these two compounds should be discarded from the analysis. When present in small quantities, their signals can be simply removed from the spectrum by digital processing.

The tissue sample collection procedures presented here describe the process as performed at the Strasbourg University Hospitals; as of this date, corresponding procedures from other clinical environments have not been described in the published literature. However, sample storage is very similar across laboratories active in this field (40,50).

2. Sample Preparation

To eliminate the risk of sample cross-contamination and cleaning issues, biopsy samples are now routinely prepared in disposable inserts. These inserts are made of polychlorotrifluoroethylene (PCTFE), marketed as KelF (Daikin Industries, Osaka, Japan), and have an active volume of about 30 μL. This volume is sufficient to accommodate 15 to 20 mg of tissue and 10 μL of D_2O. There is no need to use a buffer for biopsy studies because the physiological salts naturally present in biological tissues already provide sufficient buffering capacity. To prevent as much as possible sample degradation during the preparation procedure, samples should be prepared in the frozen state inside a cryostat regulated at −20°C (Figure 23.4). This type of equipment is routinely used in histopathology departments for the preparation of histological sections. The amount of specimen used for each sample (~15 mg) and the time required for preparation should be kept as constant as possible for all samples involved in a particular study, which is greatly facilitated by the use of biopsy punches. Because it is important to know the exact amount of tissue used in each analysis, the insert should be weighed before and after filling. Once the specimen is introduced and weighed, D_2O is added for the purpose of locking the spectrometer during the NMR experiment. After the insert has been closed with a plug, it is stored back in the −80°C freezer. At the time of analysis, the insert is

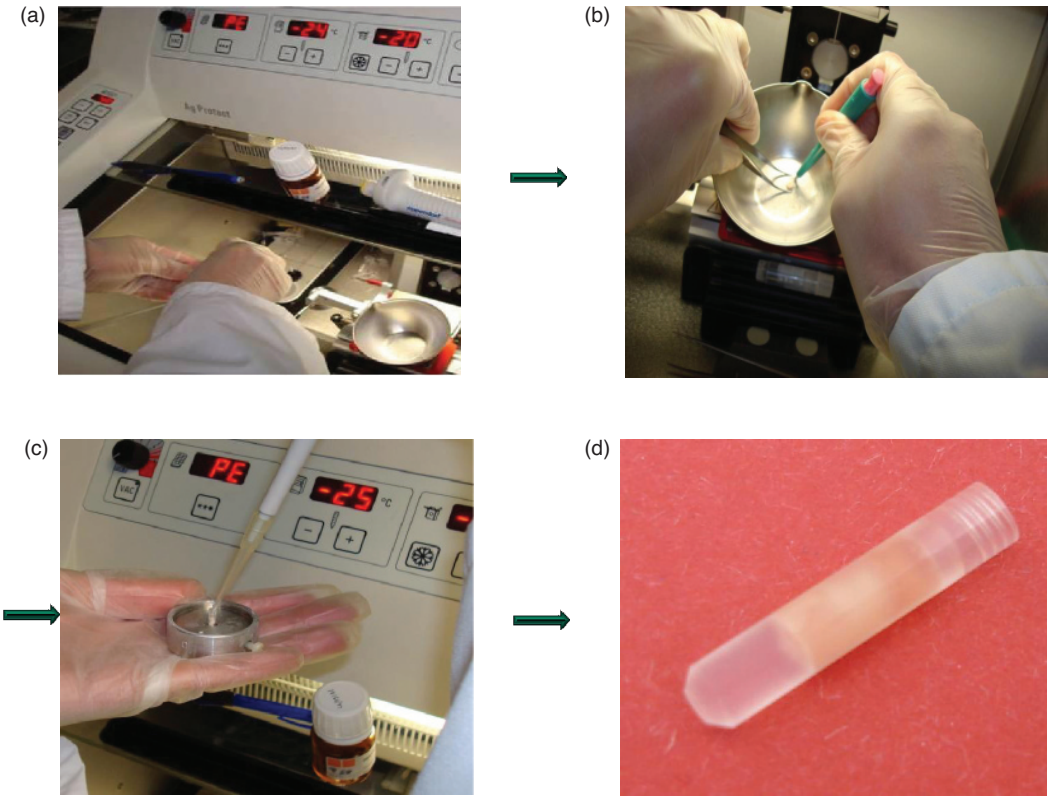

Figure 23.4. Biopsy sample preparation for HR-MAS studies. (a) Cryostat at −20°C. (b) Biopsy punch used to take the biopsy specimen. (c) Introduction of the biopsy specimen and D_2O into the insert. (d) Final insert closed with a transparent conical plug.

placed in a standard 4-mm ZrO_2 rotor of the type classically used for solid-state NMR studies (3). To obtain reproducible sample preparation, this task should be entrusted to a meticulous person who performs this preparation on a routine basis. The entire sample preparation process takes only 2 to 3 minutes for a trained person, minimizing sample degradation. At a later stage of development, automatic sample preparation procedures should be considered. Advantages of a disposable insert are that the tissue sample can be stored back in the −80°C freezer after HR-MAS analysis without the need for removing it from its recipient and that the rotor itself can be immediately reused for subsequent analyses. The biopsy specimen is available for histopathological analysis if needed. This is an important point because HR-MAS and histopathological analysis both can be performed on the same sample in cases where it is uncertain whether the mirror sample represents the same type of tissue that has been used for obtaining the metabolic data. At the present stage of development, histology on the very samples that have been used in HR-MAS experiments is not performed on a routine basis because cutting the insert to generate 5-μm slices suitable for histopathological analysis takes an extra amount of time. For this reason, the use of mirror samples cannot entirely be replaced by post–HR-MAS histology at this time.

In addition to our laboratory, these sample preparation techniques have been implemented by numerous groups working in this field (40,50). However, slight variations can be found. Some authors, instead of adding pure D_2O to the biopsy sample, prefer a solution of phosphate-buffered saline (PBS) in D_2O (16). The advantage of this approach is twofold. First, the liquid being in direct contact with tissue material is isoosmotic; this may be beneficial to tissue integrity by minimizing osmotic pressure. In this way, metabolite leakage from the tissue may be prevented or at least reduced. Second, the buffering capacity of the liquid surrounding the tissue is increased, facilitating the maintenance of constant, tissue-like pH. However, the overall salt content of the sample is increased with PBS/D_2O versus D_2O alone. This may result in a reduction of the sensitivity of the NMR experiment.

3. Data Acquisition

Before running an HR-MAS analysis of biopsy samples, one should ensure that the spectrometer is operational and meets certain specifications. First, the temperature existing inside the rotor should be calibrated precisely for the spinning speed to be used subsequently for tissue HR-MAS because samples are being heated owing to rotation (51). A calibration sample consisting of 100% MeOH or 99.8% MeOD/0.2% MeOH (52). allows high-precision temperature calibration. Because sample degradation is always of prime concern, low temperatures are mandatory, and a value of 4°C is typically chosen. This temperature ensures that tissue samples are not frozen during HR-MAS analysis.

The spinning speed is usually chosen to be as low as possible to prevent sample degradation secondary to the centrifugal forces induced by rotation. At 500-MHz measurement frequency (11.7T magnetic field), a spinning speed of 3,500 Hz (corresponding to 7 ppm) is adequate. This value is sufficiently high to prevent spinning side bands associated with the rotation to fall in the crucial 4.7- to 0.5-ppm region. For different magnetic fields or when using a wider chemical shift range for metabolite analysis, the spinning speed should be adjusted as needed. Although higher spinning speeds can be technically achieved, it is advisable to limit these to the minimum required because the risk of tissue alteration significantly increases with spinning speed. This effect not only may adversely influence the reproducibility of HR-MAS spectra, but also has detrimental consequences for tissue histology on samples that have undergone HR-MAS spectroscopy.

To obtain spectra with the required quality, the magic-angle setting (54.7 degrees) should be set precisely because it has a direct influence on the line shape of the samples (51). The standard procedure is to use a KBr sample and acquire ^{79}Br spectra. The intensity of the spinning side bands in the ^{79}Br spectrum is maximized by adjusting interactively the position of the stator. Once the magic angle is set, the quality of the shims should be checked by using a test sample containing 1% $CHCl_3$ in acetone-D_6. It is important to position the probe in the magnet in such a manner that the stator containing the radiofrequency coil is aligned either along the *x*- or the *y*-axis of the shim system of the spectrometer. This procedure allows one to decrease the number of active shims and facilitates the shimming procedure. More information concerning the exact spinning angle adjustment procedure can be found elsewhere (51). Typical full width at half height (FWHH) values of the

Table 23.1. *Standard acquisition and processing parameters for a one-dimensional CPMG experiment used at a field strength of 500 MHz for a standard biopsy sample of 15 mg (pulse program,* cpmgpr1d*, and acquisition mode,* baseopt*)*

1-D CPMG	
Acquisition Parameters	
Temperature	4°C
Rotation speed	3,500 Hz
Relaxation delay	2 sec
Acquisition time	2.34 sec
90° pulse width	About 8 μsec
Receiver gain	128
Sweep width	14 ppm
Number of scans	128
Dummy scans	4
Number of points (real + imaginary)	32k
Length of CPMG	93 msec
Interpulse CPMG delay	286 μsec
Field strength used for water presaturation	50 Hz
Experiment time	10 min
Processing Parameters	
Number of points (complex)	64k
Exponential broadening	0.3 Hz
Baseline correction	Linear

Note. The parameters used for the acquisition of a simple "90° pulse-acquire" experiment (pulse program, *zgpr*) are identical except for the absence of CPMG-specific parameters (names of pulse programs and acquisition modes are given in italics as used in Bruker instruments; similar software is available for spectrometers from other manufacturers).

$CHCl_3$ line at 7.24 ppm should be less than 1 Hz. Once acceptable values have been obtained on the $CHCl_3$ test sample, biopsy specimens can be analyzed. If the probe is positioned along the *y*-axis of the shim system, only a small set of shims (Z, Y, YZ, X2–Y2) (51) has to be adjusted for each individual biopsy sample, by optimizing the FWHH of either the lactate resonance at 1.33 ppm or the alanine resonance at 1.48 ppm. The FWHH of each doublet peak should be inferior to about 1.5 Hz. At the present time, gradient-based methods (53–55) are not yet available for automatic shimming of samples spinning at the magic angle; however, these methods are under development and should become available in the near future.

For metabolic analysis of tissue samples, 1D ^{1}H NMR data are typically recorded using either a CPMG (Carr-Purcell-Meiboom-Gill) (41) sequence or an experiment employing a simple 90-degree pulse, both with water presaturation. A solvent signal suppression sequence frequently used in the field of biofluid metabolomics is 1D ^{1}H NOESY with presaturation, which also efficiently minimizes broad signals of exchangeable protons (typically urea contained in urine). However, the advantage of ^{1}H 1D CPMG over 1D ^{1}H NOESY is that the CPMG sequence reduces the broad signals originating from proteins and lipids contained in biopsy specimens. Without attenuation, lipid signals might easily dominate the tissue spectrum, obscuring metabolite signals of interest. Acquisition parameters of a typical ^{1}H 1D CPMG biopsy tissue experiment are presented in Table 23.1. The interpulse

delay between the 180-degree pulses of the CPMG pulse train is synchronized with sample rotation (ω_r), and is set to 286 μsec ($1/\omega_r = 1/3{,}500 = 286$ μsec) to eliminate signal losses owing to B_1 field inhomogeneity (56,57). The number of loops (i.e., 180-degree pulses) is typically set to 328, yielding a total CPMG pulse train length of 93 msec. This value is adequate to reduce the intensity of lipid signals to the level of the metabolites in most organs (i.e., brain, colon, kidney, and ovary). For samples originating from organs containing large amounts of lipids, such as breast, the length of the CPMG pulse train should be increased to 200 to 250 msec (58). Metabolite signal intensities are reduced owing to the presence of the CPMG sequence preceding data acquisition, and this attenuation depends on the length of the CPMG pulse train (i.e., effective echo delay [TE]). However, the signal attenuation secondary to a given echo delay decreases with increasing transverse relaxation time (T_2) of the observed protons, where $T_2 = 1/(LW*\pi)$, with LW being the natural linewidth of the corresponding peak ($LW \leq FWHH$).

With our current protocol, the lines generated by virtually all metabolite molecules are relatively narrow (1 to 1.5 Hz), which indicates that the lower limit for T_2 is approximately 210 msec. The "true" T_2 values should be significantly higher because factors such as residual magnetic field inhomogeneity effects also contribute to the measured linewidth, FWHH. Therefore, no dramatic signal attenuation is to be expected for the metabolites in question when a relatively short CPMG pulse train is employed (e.g., the pulse train length of 93 msec mentioned previously). Because all metabolite resonances exhibit roughly similar linewidths, the signal attenuation secondary to the CPMG pulse train is similar for all metabolites (provided that the actually observed linewidths are not strongly influenced by residual magnetic field inhomogeneities). It is also implied that the relative metabolite concentrations would not be substantially affected by the length of the CPMG pulse train (i.e., pulse train effects would be within the narrow limits indicated by linewidth variations). The same argument holds for the determination of absolute concentrations provided that the spectrum of the metabolite in the reference solution is recorded under the same CPMG conditions that are applied to the tissue samples.

The data acquisition time for each FID is set to 2.34 seconds to provide adequate resolution, and the recycling delay is set to 2 seconds to obtain pseudoquantitative spectra within an acceptable measurement time. Significantly longer recycling delays would be needed to avoid any signal saturation secondary to incomplete longitudinal relaxation of the protons of many metabolites ($TR \geq 5*T_1$, where T_1 is the longitudinal relaxation time of the protons in question, and TR is the repetition time for each scan – the sum of the data acquisition time and the recycling delay). However, such delays would result in prohibitively long spectrum acquisition times. Saturation effects must be considered for exact determinations of absolute metabolite quantities based on this protocol.

Typically, 128 scans are acquired, resulting in a total measurement time of 10 minutes. These conditions provide an adequate signal-to-noise ratio and fast turnover and minimize tissue degradation effects; the latter become particularly significant when the overall sample spinning time exceeds 30 minutes. To automate the acquisition process as much as possible and to avoid unnecessary adjustments, the receiver gain of the spectrometer is kept at a constant value (Table 23.1). The only

parameter individually adjusted for each sample is the 90-degree pulse width. This parameter varies slightly among samples and can affect absolute quantification of metabolites. Further details concerning quantification are mentioned in section 5 on data analysis and signal assignment.

In essence, the data acquisition protocol is common to virtually all laboratories analyzing human biopsy samples (40,50). Nonetheless, minor variations in experimental parameters have been reported. For example, although it is now accepted that low temperatures should be used for the acquisition of biopsy sample spectra, temperature values ranging from 1°C to 4°C have been published. The length of the CPMG pulse train varies between 50 msec and 250 msec, depending on the project described. This variation can be explained by the fact that this parameter is organ-dependent, and its optimal value depends on the amount of lipid present in the tissue. The exact values used for TR, the data acquisition time, and the interpulse delay of the CPMG pulse train also may differ slightly from the values presented in the protocol described.

4. Data Processing

All 1D ^{1}H CPMG spectra should be recorded in such a manner that only zero-phase order correction is necessary to phase the spectrum properly (Table 23.1). The first-order phase correction is close to zero for all spectra. This procedure generates spectra with fairly flat baselines and offsets close to zero. The FID is multiplied by an exponential weighting function corresponding to a line broadening of 0.3 Hz before Fourier transformation (Table 23.1). At the present time, spectra are processed using an automatic baseline correction routine employing a simple linear correction to obtain a baseline level that is exactly at 0. ^{1}H spectra are referenced by setting the lactate doublet chemical shift to 1.33 ppm. TSP is an unreliable reference for chemical shift referencing because it can bind to various proteins or membranes in the sample, making its chemical shift sample dependent. In the event of the presence of contaminants such as OCT or ethanol at low concentrations, digital processing of the spectra can be used to set the intensity of the corresponding spectral regions to zero.

Although most laboratories use data processing methods very similar to those presented in this chapter (40,50), the reference compound, lactate, is replaced in some protocols with a different metabolite, such as alanine (1.48 ppm) or glucose (5.23 ppm) (59).

5. Data Analysis and Signal Assignment

Specific experiments used for the assignment of metabolites present in biopsy samples are primarily ^{1}H/^{13}C HSQC, and DIPSI2 sequences. Measurement times for each of these experiments are typically 8 and 15 hours, respectively. Because the duration of these experiments is long, they are acquired on only a few samples that are representative of each class of tissues and exclusively for the purpose of signal assignment. Significant tissue degradation occurs during this long measurement time; therefore, ^{1}H CPMG experiments have to be completed before these signal assignment experiments. Further assignment methods are described in Chapter 24.

In addition, assignment of spectral resonances can be facilitated by using published literature values or specific databases (e.g., Human Metabolome Database (60) or Bruker Metabolic Database). For most biopsy samples, 35 to 45 metabolites are detected. Greater than 90% of the metabolites detected by ^{1}H HR-MAS NMR are common to all organs. Specific metabolites are more abundant in the brain (NAA, GABA), the adrenal gland (epinephrine) (28), or the prostate (citrate) (22). Quantification of metabolites in each sample is of paramount importance because metabolic profiling potentially reveals characteristic values for sets of metabolites for many healthy and cancerous tissues. With current technology, it is possible to detect by HR-MAS NMR approximately 35 to 45 metabolites in about 15 mg of tissue within an experimental time of about 10 minutes. This corresponds to a detection threshold of about 0.1 mmol of metabolite per kilogram of tissue. Because magnetic resonance is an intrinsically quantitative technique, it is possible to obtain exact absolute metabolite levels for each sample, provided that signal saturation effects are taken into consideration or are avoided altogether. The influence of acquisition parameters on signal intensities is discussed in section 3 on data acquisition. The quantitation technique suggested in this protocol includes calibration by separately measuring the signal intensity of a reference solution containing a known amount of a metabolite, typically lactate, under exactly the same conditions used for the measurement of biopsy samples. We have found that the T_1 values measured in these reference solutions were similar to the corresponding values in tissue samples (data not published). In cases where precise absolute quantitation is needed, correction for saturation has to be included as mentioned in section 3. The fact that CPMG linewidths are also similar in reference solutions and in tissue indicates that any signal attenuation owing to the CPMG pulse train (effective TE) should be similar in both sample types. The recommended quantitation method with the aid of reference solutions provides a good approximation at this stage of development. In addition, a technique using an electronic reference signal for quantitation (Eretic ["electronic reference to access in vivo concentrations"] (61)) associated with a method based on pulse length measurements (PULCON ["pulse length based concentration"] (62)) is particularly powerful (63). The current state-of-the-art Eretic method is a digital version that does not require any additional hardware but only a dedicated program that digitally adds a synthetic reference signal to the NMR spectrum.

At the present time, only peaks that are well resolved in 1D CPMG spectra can be routinely quantified. However, using more sophisticated methods such as LCModel (LCModel Inc., Oakville, Canada) (64) or jMRUI (University of Lyon, Lyon, France) (65), it will eventually be possible to quantify larger sets of metabolites. These advanced techniques have the added advantage of taking into account the entire spectra of all metabolites in the quantitation process, which significantly reduces the probability of overestimating certain metabolite levels owing to "invisible" peaks that may lie under the resonances to be quantitated. This is a common problem in all biological 1D proton spectra. In addition, this software allows one to include model spectra of macromolecules and lipids. These compounds generate very broad resonances that effectively "deform" the baseline, even though CPMG protocols reduce their appearance. Current routine baseline correction methods neglect these effects, which may result in further overestimation of certain metabolite levels. Methods such as LCModel or jMRUI will be recommended for use in

clinical routine protocols once they are able to process large quantities of spectra rapidly and automatically. By and large, the data analysis and signal assignment techniques described in this chapter have found numerous applications in the field of biopsy sample HR-MAS NMR spectroscopy (40,50).

6. Statistical Analysis

In most cases, the spectral region between 4.7 ppm and 0.5 ppm of each 1D ^{1}H CPMG NMR spectrum is automatically subdivided into regions of 0.01 or 0.001 ppm width for automated statistical evaluation. This process is also known as "binning" or "bucketing." If necessary, the region between 10 ppm and 5.2 ppm can also be used for the analysis. However, the region containing the residual water signal at approximately 5 ppm is systematically excluded. A large variety of manufacturers provide software platforms that can be used for binning; these platforms can be programmed by users or are programmed by the manufacturer to perform this task. Examples shown in this chapter are based on AMIX software (Bruker Biospin, Rheinstetten, Germany).

The widths of the bucketing regions can be adjusted to minimize effects of peak shifts owing to variations in pH or salt content. The choice between 0.01 ppm or 0.001 ppm bucketing depends on how well corresponding peaks in the spectra to be compared are aligned. The quality of peak alignment can be assessed easily by inspecting the stacked plots of the spectra to be included in a specific statistical evaluation. The peak integral within each individual bucket region is computed with the aid of AMIX or with a MatLab-based program and normalized with respect to the total integral of the entire spectral region included (typically 4.7 to 0.5 ppm). This procedure allows normalizing all metabolite signals of a given spectrum to tissue sample weight. If necessary, signals originating from contaminants or lipids can also be removed at this stage by excluding the corresponding spectral regions from the bucketing and normalization processes. The bucketing process generates an X data matrix with a number of columns corresponding to the number of buckets and a number of rows corresponding to the total number of samples used.

Data sets are imported into a statistics program for analysis (e.g., SIMCA P 11.0 software from Umetrics AB, Umeå, Sweden). First, data are preprocessed to give equal weight to metabolites present at high and low concentrations. Then, data are first analyzed using principal component analysis (PCA) (66,67). This unsupervised multivariate data reduction routine serves to evaluate the quality of the data quickly and to identify possible outliers. In the typical case of a two-group study, the two groups first should be subjected to independent PCA analyses. Outliers in each group might be due to incorrect spectral referencing, poor data quality (e.g., because of suboptimal shims, phase errors), or occasionally the presence of contaminating signals (e.g., chemical impurities, electronic "parasites") that were not removed at an earlier stage of spectrum processing This procedure is very useful for identifying samples that are contaminated with ethanol or fixing agents. Spectra from these contaminations usually appear unmistakably in the score plot of the first two principal components. The spectra of these outliers should be inspected visually and either corrected or removed from the analysis. After PCA analysis, a supervised partial least square discriminant analysis (PLS-DA) (67–69) is usually

employed to build a statistical model that optimizes the separation between the two groups. The number of components of the PLS-DA model is determined by cross-validation. The class membership of each sample is iteratively predicted, using the results to generate a goodness-of-fit measure, Q^2, for the overall model. The maximum theoretical value for Q^2 is equal to 1 for perfect prediction. However, a Q^2 value more than 0.5 is generally considered to be a decent predictor. Because in practice PLS-DA models are often built using a relatively small number of samples compared with the number of variables, an extensive cross-validation of the model is mandatory to avoid overfitting of the data (70).

The combination of PCA and PLS-DA has become the universally used standard approach to this type of analysis (40,50). However, more sophisticated statistical methods such as hierarchical cluster analysis, K–nearest neighbor analysis, or neural networks are also in use (71). Further details of statistical methods can be found in Chapters 4 through 10.

7. Sample Reproducibility in High-Resolution Magic Angle Spinning

When studying cohorts of humans by tissue HR-MAS, it is essential to ensure a high level of reproducibility for all samples belonging to a specific group, for all groups. This includes separate validation for control (healthy) and diseased tissues because the two might behave slightly differently with respect to reproducibility. While setting up a statistical model, detailed histopathological results should be available for all samples to ascertain the exact characteristics of the tissue type in question. The contribution of histopathologists is crucial at all stages of the study. In this section, we present two examples of reproducibility studies based on different human tissues.

7.1. Epilepsy

Thirty-seven 1D ^{1}H CPMG spectra of healthy human cerebral cortex were obtained from patients with epilepsy who had undergone surgical removal of the hippocampus (Figure 23.5). This set of spectra shows convincingly that the protocol described in this chapter can be used to obtain highly reproducible brain tissue spectra. Because no normalization with respect to sample weight was applied for the display of these spectra, the globally constant signal intensities across all spectra indicate that the weight of biopsy specimens was rather constant. Sample contamination by ethanol is visible in some spectra (peaks at 1.18 ppm and 3.65 ppm). Because these contaminations were not very large, the corresponding spectral regions were simply set to zero in all the spectra for statistical evaluation. The corresponding PCA analysis is shown in Figure 23.6. Only the first two principal components of the PCA model are shown because they account for the largest variability in the sample. In this example, the first and the second component (PC1 and PC2) account for 18% and 14% of the variability. Most of the spectra fell within the Hotelling T2 ellipse shown, with a confidence level of 95%. Only two data points fell outside the T2 ellipse. The corresponding outlier spectra showed slightly abnormal intensities at 2.19 ppm and 3.5 ppm, which probably explain the nontypical behavior of the two points in the PCA plot.

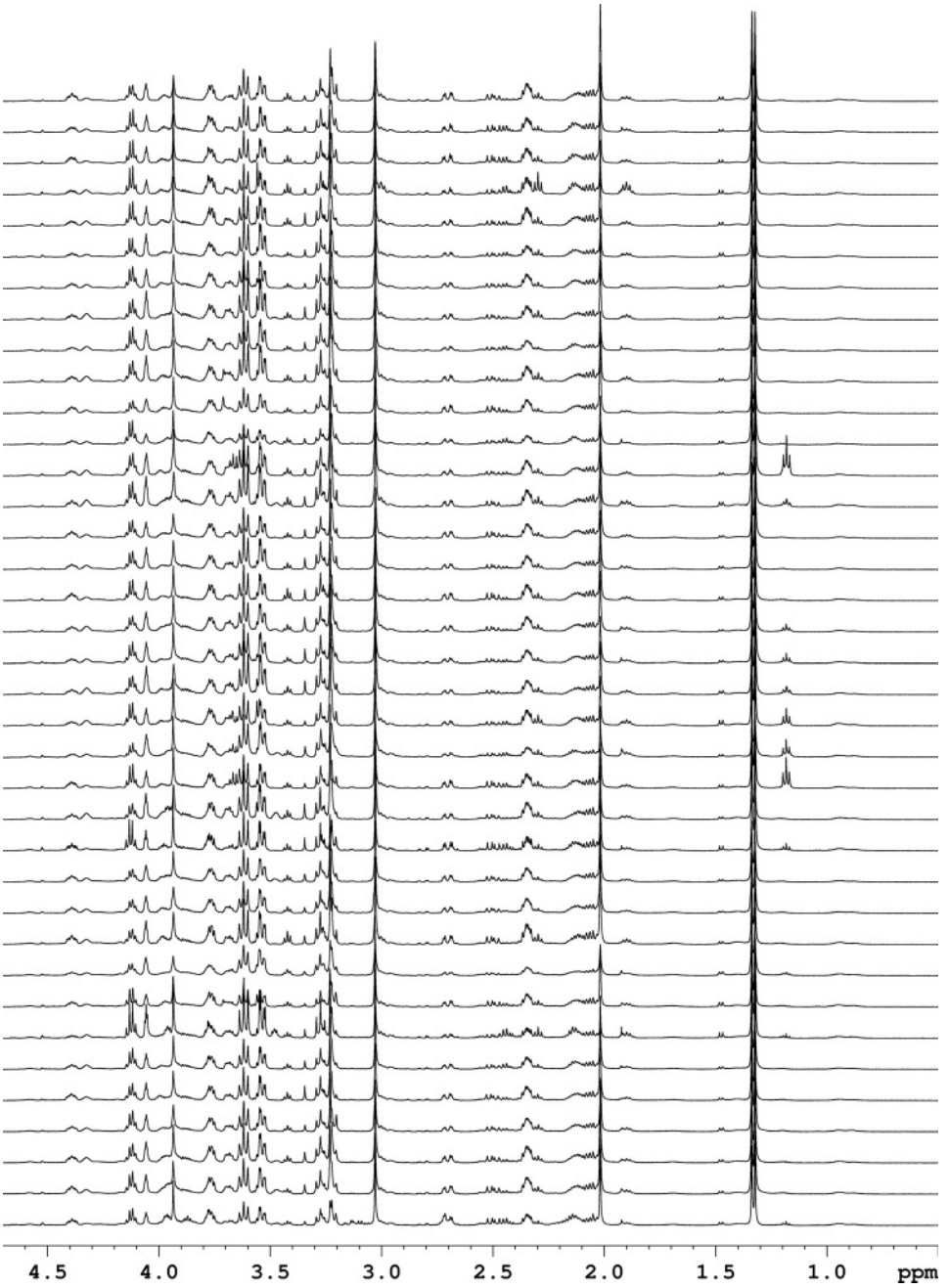

Figure 23.5. Stacked plot of 1D ^{1}H HR-MAS CPMG spectra of healthy human cortex biopsy specimens originating from thirty-seven different patients.

7.2. Normal Kidney Tissue and Renal Cell Carcinoma

1D ^{1}H CPMG spectra of healthy kidney and renal cell carcinoma biopsy samples were acquired, originating from twenty different patients. Clear or conventional renal cell carcinomas represent 75% to 80% of renal cell carcinomas, the latter accounting for about 90% of adult renal tumors (72–74). From each patient,

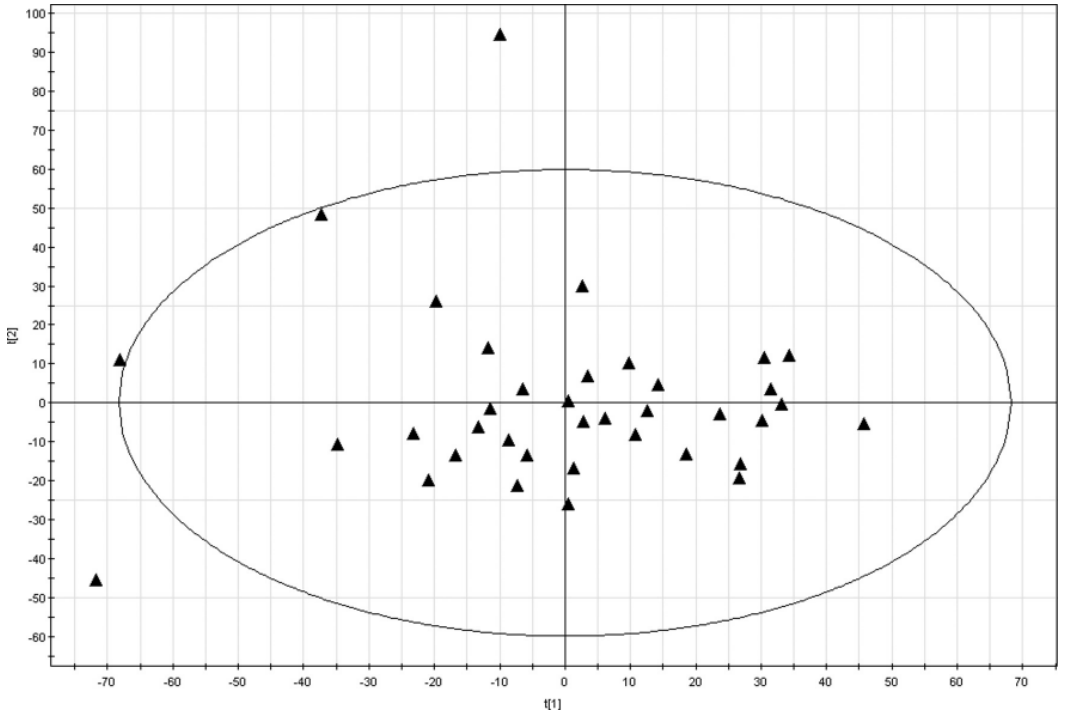

Figure 23.6. PCA analysis of the spectra shown in Figure 23.5 corresponding to thirty-seven healthy human cortex biopsy specimens (spectral region corresponding to the ethanol resonances set to zero).

one healthy and one cancerous biopsy specimen were taken. The data presented in Figure 23.7 show the reproducibility of these spectra across the patient cohort (ethanol contamination is observable for several samples). Visual inspection of these spectra immediately reveals the existence of differences in metabolic signatures between control and clear renal cell carcinoma tissues. The cancerous samples are clearly characterized by a conspicuously intense lipid peak at 0.9 ppm. Table 23.2 presents detailed assignments of metabolites detected in healthy kidney tissue.

To ascertain further the reproducibility of the method, the average concentration of selected metabolites was evaluated for the twenty healthy human kidney samples presented in Figure 23.7. Metabolite concentrations were obtained from each spectrum by simply integrating the areas under individual peaks representing the resonances of the metabolites being analyzed. Only metabolites presenting at least one resonance with sufficient spectral resolution were selected for this analysis. A more robust but also more time-consuming protocol using the software LCModel (64) or jMRUI (65) would lead to more reliable results (see section 5 on data analysis and signal assignment). Nevertheless, the results presented in Table 23.3 show very reasonable standard deviations for the metabolite concentrations evaluated.

The corresponding PCA analysis of these two sets of spectra, based on 0.01-ppm bucketing, is shown in Figure 23.8. Only the first two principal components of the PCA model are shown because they account for the largest variability in the sample. For the cancerous tissue samples (Figure 23.8(a)), PC1 and PC2 account for 19% and 9% of the variability. This data set is unusually large and contains 139

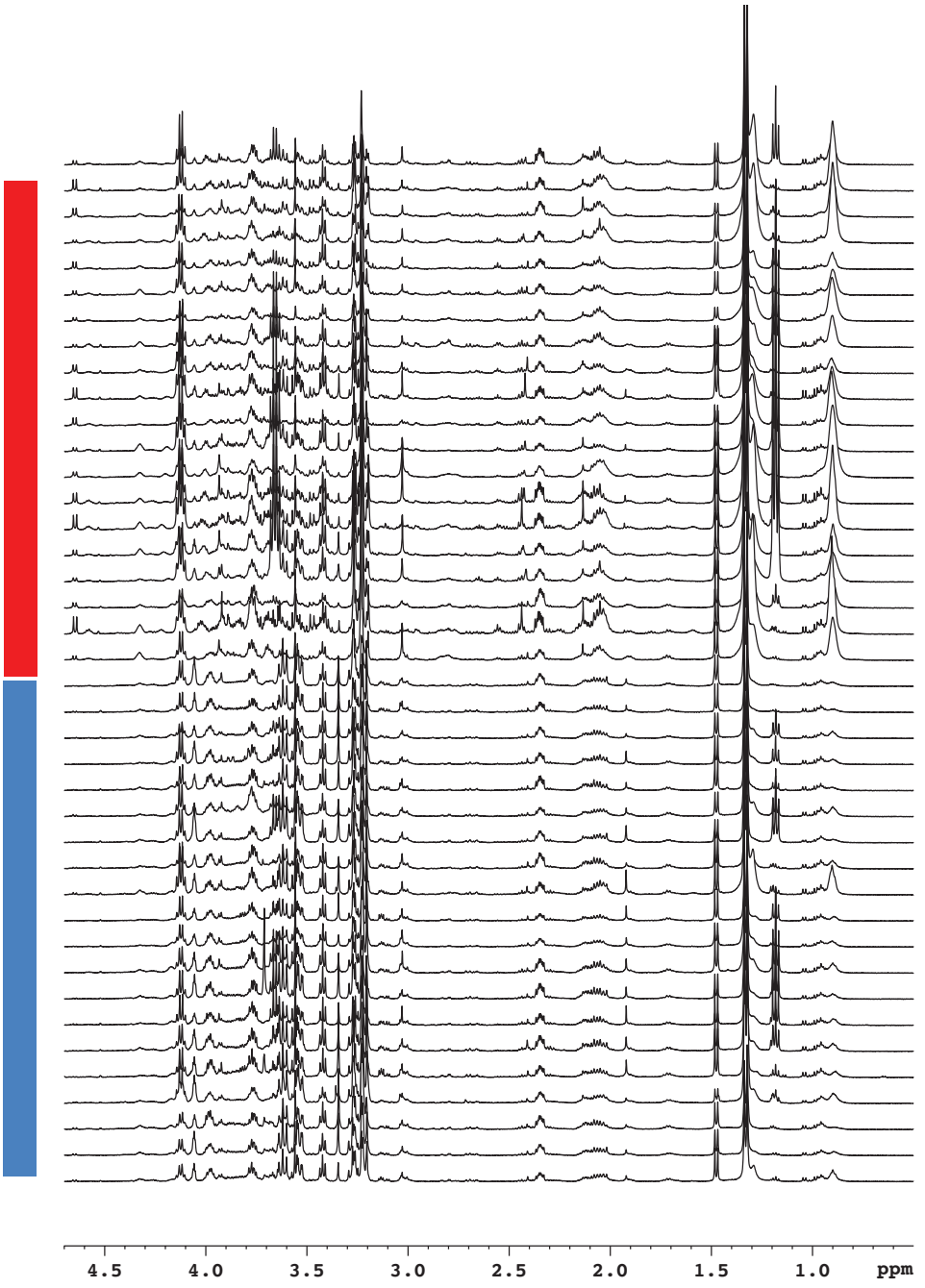

Figure 23.7. Stacked plot of 1D HR-MAS CPMG spectra of control kidney biopsy samples (*blue*) and clear renal cell carcinoma tissue (*red*).

spectra. As in the previous example (section 7.1 on epilepsy), most of these spectra fell within the Hotelling T_2 ellipse. Only four data points fell slightly outside the T_2 ellipse. For the corresponding control tissues (Figure 23.8(b)), PC1 and PC2 account for 19% and 14% of the variability (119 spectra; 9 outside the T_2 ellipse).

Table 23.2. *^{1}H and ^{13}C resonance assignment of metabolites present in healthy human kidney biopsy specimens*

Metabolites	Group	^{1}H Chemical shift (ppm)	^{13}C Chemical shift (ppm)
Acetate	CH_3	1.92	25.97
Alanine	βCH_3	1.48	18.81
	αCH	3.78	53.22
Arginine	αCH_2	1.70	26.75
	αCH_2	1.92	30.15
	δCH_2	3.21	43.27
Ascorbate	$CH_2(OH)$	4.02	72.12
	C_4H	4.52	81.25
Asparagine	CH	4.00	54.15
	CH_2	2.94	37.43
	CH_2	2.84	37.35
Aspartate	CH_2	2.70	39.17
	CH_2	2.80	39.17
	CH_2	3.90	54.93
Choline	$N\text{-}(CH_3)$	3.21	56.75
	CH_2	3.52	69.96
	CH_2	4.06	58.27
Creatine	CH_3	3.03	39.64
	CH_2	3.93	56.36
Ethanolamine	CH_2	3.80	60.57
	CH_2	3.13	44.18
Fatty acids (a)	CH_2	1.29	34.53
	CH_2	1.31	25.36
Fatty acids (b)	CH_2	2.03	27.35
	CH_2	2.80	28.16
	CH	5.33	130.51
	CH	5.33	132.2
Fatty acids	CH_3	0.90	16.96
	$CH_2\text{-}CO$	2.25	36.43
Fatty acids (a) (b)	(n) CH_2	1.29	32.4
Fatty acids (c)	CH_2	1.60	27.3
GABA	CH_2	2.30	–
α-Glucose	C_4H	3.43	72.58
	C_1H	5.23	94.44
	CH	3.84	59.12
β-Glucose	C_3H, C_5H	3.47	78.44
	C_6H	3.75	63.44
	C_6H	3.89	63.44
	C_1H	4.65	98.7
Glutamate	CH_2	2.05	29.74
	CH_2	2.34	35.95
	CH	3.76	57.2
Glutamine	CH_2	2.14	29.52
	CH_2	2.44	33.48
	CH_2	3.77	57.38
Glycerol	$1,3CH_2OH$	3.56	65.09
	$1,3CH_2OH$	3.65	65.09
	CHOH	3.78	74.85
Glycerophosphocholine	$N\text{-}(CH_3)_3$	3.23	56.75
	αCH_2	4.32	62.19
	βCH_2	3.69	68.5

Metabolites	Group	^{1}H Chemical shift (ppm)	^{13}C Chemical shift (ppm)
Glycine	CH_2	3.56	44.09
Isoleucine	CH_3	0.94	13.79
	CH_3	1.01	17.29
	CH_2	1.51	27.30
	CH	3.65	62.34
Lactate	CH_3	1.33	22.7
	CH	4.12	71.11
Leucine	CH_3	0.95	23.43
	CH_3	0.91	24.52
	CH	1.70	26.78
	CH_2	1.70	42.37
	CH	3.73	56.06
Lysine	CH_2	1.43	24.21
	CH_2	1.71	29.10
	CH_2	1.89	32.56
Methionine	CH_3	2.12	16.61
	CH_2	2.18	32.72
	CH_2	2.64	31.50
	$CHNH_2$	3.85	56.84
Myo-inositol	C_5H	3.27	77.00
	C_1H, C_3H	3.54	73.84
	C_4H, C_6H	3.61	75.06
	C_2H	4.06	74.85
Phenylalanine	$CH_{2,6}$	7.30	131.81
	C_4	7.37	131.49
Phosphocholine	$N(CH_3)_3$	3.22	56.52
	CH_2	3.60	68.98
	CH_2	4.16	60.60
Phosphoethanolamine	CH_2	3.98	63.05
	$CHNH_2$	3.22	43.35
Proline	CH_2	3.32	48.83
	CH_2	3.41	48.83
	CH	4.10	64.39
Scyllo-inositol	All HS	3.35	76.32
Serine	CH	3.84	59.12
	CH	3.97	62.88
Taurine	CH_2-NH_3	3.26	50.13
	CH_2-SO_3	3.42	38.06
Threonine	CH	3.60	63.04
	CH	4.24	68.67
	CH_3	1.32	22.30
Tyrosine	CH	3.92	58.72
	$CH_{3,5}$	6.87	118.50
	$CH_{2,6}$	7.16	133.37
Valine	CH_3	0.98	19.16
	CH_3	1.04	20.65
	CH	2.30	31.94

Note. The nomenclature used for fatty acids is defined by Martínez-Bisbal et al. (15).

Table 23.3. *Average concentrations and standard deviations of selected metabolites present in healthy human kidney biopsy specimens*

Metabolites	Average concentration (mmol*kg^{-1})	Standard deviation
Acetate	0.46	0.12
Alanine	1.69	0.31
Ascorbate	0.20	0.06
Asparagine	6.08	0.95
Aspartate	0.71	0.18
Choline	0.70	0.14
Ethanolamine	0.67	0.15
Glutamate	2.43	0.53
Glutamine	0.46	0.10
Glycine	3.50	0.52
Lactate	7.15	1.83
Lysine	1.10	0.16
Myo-inositol	3.94	1.21
Scyllo-inositol	2.62	1.14
Taurine	2.71	0.35
Valine	0.21	0.04

8. Metabolic Tissue Profiling by High-Resolution Magic Angle Spinning Nuclear Magnetic Resonance Spectroscopy

The purpose of clinical metabolic tissue profiling is to gain information on the metabolic pathways active in different tissues and for different pathologies and to establish correlations between the patients' metabolic data and their clinical evolution. This is particularly important for pathologies and patients where a discrepancy exists between histopathological diagnosis and clinical evolution. Some promising results for human brain tumors have appeared more recently in the literature (14). These results show that for some intermediate oligodendroglioma and glioblastoma cases, metabolic results are better correlated with the evolution of the patient than the corresponding histopathological data. These results are preliminary and need to be confirmed by complementary studies; however, they already open very interesting perspectives. As a first step, being able to differentiate healthy tissue from apparently healthy tissue infiltrated by cancer cells is an important issue; this is not only interesting from a biological point of view but also for possible applications such as real-time metabolic analysis of tissues in the context of a surgical operation (83). This type of application, if validated clinically, could be of great importance in the case of brain surgery because it would allow the surgeon to delineate exactly the tumorous part of the tissue. Figures 23.8 and 23.9 illustrate the potential of future applications of the procedures described in this chapter to tissue metabolic profiling. Simple PLS-DA analysis of the kidney data (Figure 23.8) proves that distinction between healthy and cancerous kidney tissues can be readily achieved. The PLS-DA score plot of the two principal components shows clear separation between the two sets of data (Figure 23.9). Numerous results published in the literature prove that this methodology can be successfully applied to several different organs. Particularly promising results have been obtained for prostate (22,75,76), breast

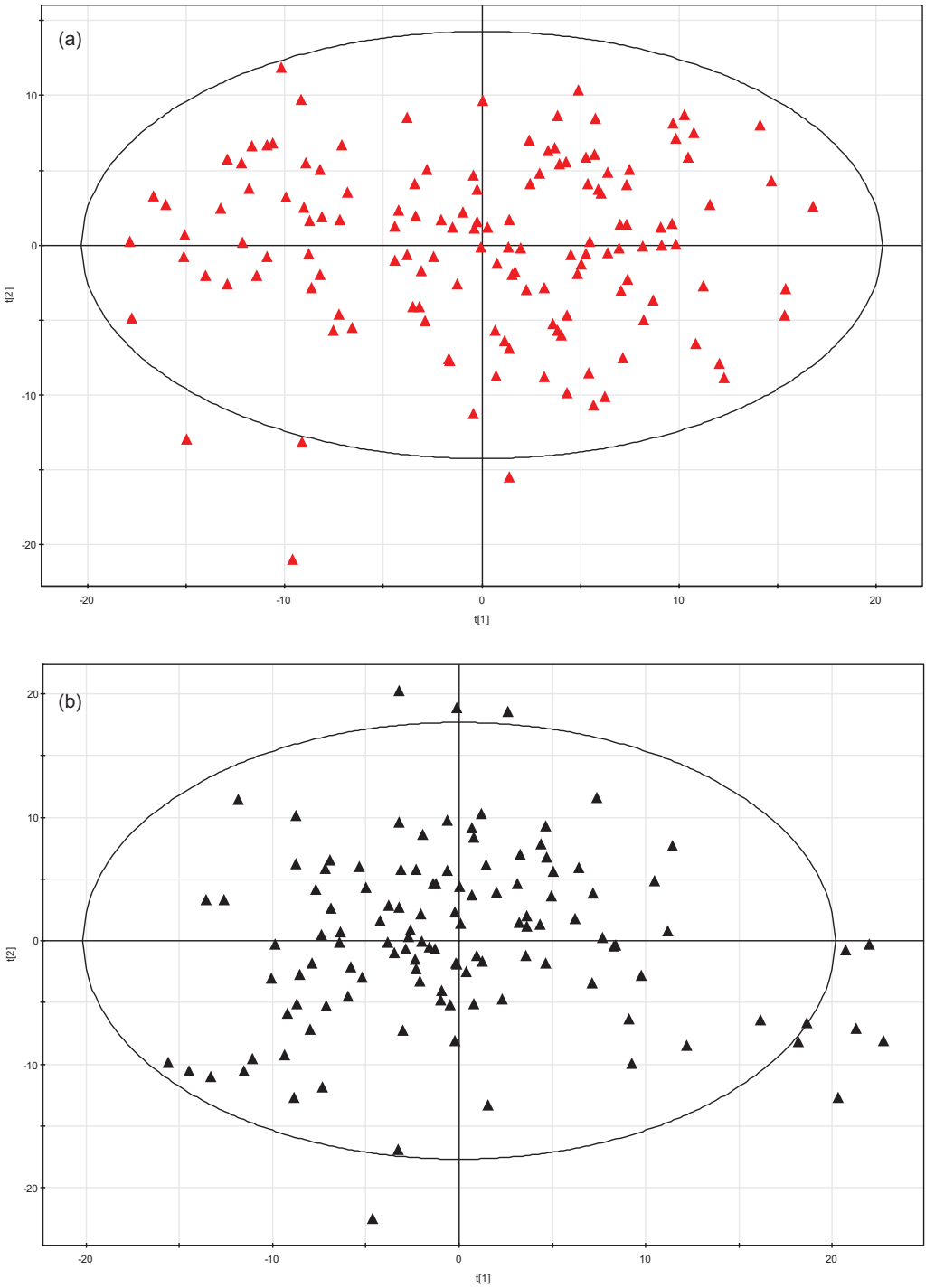

Figure 23.8. Principal component analysis of control (a) and clear cell adenocarcinoma (b) kidney tissue, based on 1D HR-MAS CPMG spectra (see also Figure 23.7).

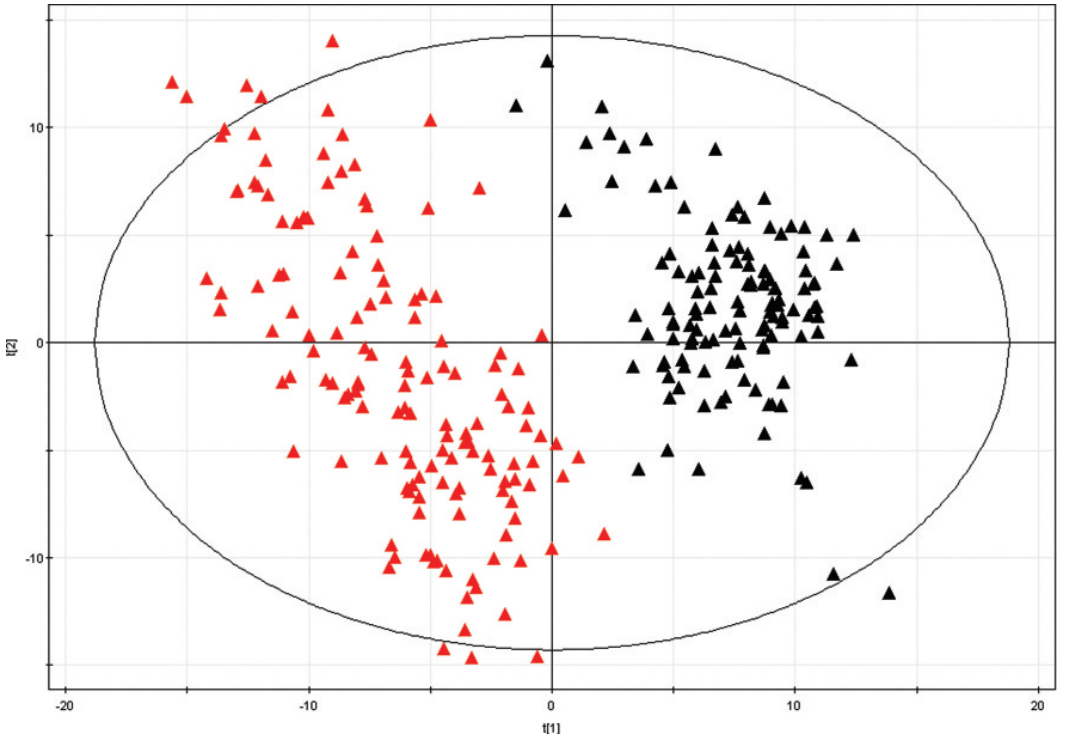

Figure 23.9. PLS-DA analysis of control kidneys (*black triangles*) and clear renal cell carcinoma kidney biopsy specimens (*black boxes*) (see also Figures 23.7 and 23.8).

(16,58,77), brain (13,15,78), kidney (26,27), colon (32,34,79,80), and cervical cancers (30,81,82).

9. Conclusion

Standardization of protocols for reliable tissue metabolic profiling of human biopsy samples can be achieved in such a way as to be compatible with the constraints of a hospital environment. For this purpose, numerous precautions must be taken during the whole chain of events between sample collection and statistical data analysis. Because this type of tissue analysis involves human samples, the participation of physicians and other medical personnel is crucial to the success of the procedure. The modifications of standard medical protocols that are required for robust metabolic profiling by HR-MAS are minor and should be easily implemented in many hospitals. One of the future axes of development will be the full automation of the HR-MAS measurement process. This development not only will save time and manpower but also will ensure better reproducibility of HR-MAS data. Full automation will also allow hospital laboratory personnel to perform these analyses independently. The development of refrigerated HR-MAS sample changers greatly facilitates this task. This also applies to future developments regarding automatic tuning and matching of the HR-MAS probe and automatic gradient shimming of the sample (53,55). At a later stage, dedicated robots could be envisaged to

automate the sample preparation process. Finally, when reliable statistical models representative of different tumor types and organs have been developed, these should become an integral part of medical HR-MAS spectrometers, making it possible to evaluate specific biopsy specimens in a fully automatic mode.

Acknowledgments

This work is part of the CARMeN project and was supported by grants from University Hospitals of Strasbourg, University of Strasbourg, Bruker BioSpin, Région Alsace, Oséo, Communauté Urbaine de Strasbourg, and Conseil Départemental du Bas-Rhin. The technical assistance of Dr. J. Raya, Mrs. H. Kada, and Mrs. T. Tong is gratefully acknowledged.

REFERENCES

(1) Andrew, E. R.; Bradbury, A.; Eades, R. G., Removal of dipolar broadening of nuclear magnetic resonance spectra of solids by specimen rotation, *Nature* 1958, *183*, 1802.
(2) Lowe, I. J., Free induction decays of rotating solids, *Phys. Rev. Lett.* 1959, *2*, 285.
(3) Lippens, G.; Bourdonneau, M.; Dhalluin, C.; Warras, R.; Richert, T.; Seetharaman, C.; Boutillon, C.; Piotto, M., Study of compounds attached to solid supports using high resolution magic angle spinning NMR, *Curr. Org. Chem*. 1999, *3*, 147.
(4) Filtch, W. L.; Dettre, G.; Holmes, C. P.; Shoolery, J.; Keifer, P. A., High-resolution ^{1}H NMR in solid-phase organic synthesis, *J. Org. Chem*. 1994, *59*, 7955.
(5) Anderson, R. C.; Jarema, M. A.; Shapiro, M. J.; Stokes, J. P.; Zilliox, M., Analytical techniques in combinatorial chemistry: MAS CH correlation in solvent-swollen resin, *J. Org. Chem*. 1995, *60*, 2650.
(6) Keifer, P. A., Influence of resin structure, tether lengh and solvent upon the high resolution ^{1}H NMR spectra of solid-phase synthesis resin, *J. Org. Chem*. 1996, *61*, 1558.
(7) Doskocilova, D.; Tao, D.; Schneider, B., Effects of macroscopic spinning upon linewidth of NMR signals of liquids in magnetically inhomogeneous systems, *Czech. J. Phys. B*. 1975, *25*, 202.
(8) Elbayed, K.; Furrer, J.; Raya, J.; Hirschinger, J.; Bourdonneau, M.; Richert, T.; Piotto, M., Origin of the residual NMR linewidth of a peptide bound to a resin under magic angle spinning, *J. Magn. Reson.* 1999, *136*, 127.
(9) Cheng, L. L.; Lean, C. L.; Bogdanova, A.; Wright Jr, S. C.; Ackerman, J. L.; Brady, T. J.; Garrido, L., Enhanced resolution of proton NMR spectra of malignant lymph nodes using magic-angle spinning, *Magn. Reson. Med.* 1996, *36*, 653.
(10) Cheng, L. L.; Ma, M. J.; Becerra, L.; Ptak, T.; Tracey, I.; Lackner, A.; Gonzàlez, R. G., Quantitative neuropathology by high resolution magic angle spinning proton magnetic resonance spectroscopy, *Proc. Natl. Acad. Sci. U. S. A.* 1997, *94*, 6408.
(11) Cheng, L. L.; Chang, I. W.; Louis, D. N.; Gonzalez, R. G., Correlation of high-resolution magic angle spinning proton magnetic resonance spectroscopy with histopathology of intact human brain tumor specimens, *Cancer Res.* 1998, *58*, 1825.

(12) Cheng, L. L.; Anthony, D. C.; Comite, A. R.; Black, P. M.; Tzika, A. A.; Gonzalez, R. G., Quantification of microheterogeneity in glioblastoma multiforme with ex vivo high-resolution magic-angle spinning (HRMAS) proton magnetic resonance spectroscopy, *Neuro-Oncology* 2000, *2*, 87.
(13) Tzika, A. A.; Cheng, L. L.; Goumnerova, L.; Madsen, J. R.; Zurakowski, D.; Astrakas, L. G.; Zarifi, M. K.; Scott, R. M.; Anthony, D. C.; Gonzalez, R. G.; Black, P. M., Biochemical characterization of pediatric brain tumors by using in vivo and ex vivo magnetic resonance spectroscopy, *J. Neurosurg.* 2002, *96*, 1023.
(14) Erb, G.; Elbayed, K.; Piotto, M.; Raya, J.; Neuville, A.; Mohr, M.; Maitrot, D.; Kehrli, P.; Namer, I. J., Toward improved grading of malignancy in oligodendrogliomas using metabolomics, *Magn. Reson. Med.* 2008, *59*, 959.
(15) Martínez-Bisbal, M. C.; Martí-Bonmati, L.; Piquer, J.; Revert, A.; Ferrer, P.; Llácer, J. L.; Piotto, M.; Assemat, O.; Celda, B., ^{1}H and ^{13}C HR-MAS spectroscopy of intact biopsy samples ex vivo and in vivo 1H MRS study of human high grade gliomas, *NMR Biomed.* 2004, *17*, 191.
(16) Sitter, B.; Lundgren, S.; Bathen, T. F.; Halgunset, J.; Fjosne, H. E.; Gribbestad, I. S., Comparison of HR MAS MR spectroscopic profiles of breast cancer tissue with clinical parameters, *NMR Biomed.* 2006, *19*, 30.
(17) Sitter, B.; Sonnewald, U.; Spraul, M.; Fjosne, H. E.; Gribbestad, I. S., High-resolution magic angle spinning MRS of breast cancer tissue, *NMR Biomed.* 2002, *15*, 327.
(18) Gribbestad, I. S.; Sitter, B.; Lundgren, S.; Krane, J.; Axelson, D., Metabolite composition in breast tumors examined by proton nuclear magnetic resonance spectroscopy, *Anticancer Res.* 1999, *19*, 1737.
(19) Borgan, E.; Sitter, B.; Lingjærde, O. C.; Johnsen, H.; Lundgren, S.; Bathen, T. F.; Sørlie, T.; Børresen-Dale, A.; Gribbestad, I. S., Merging transcriptomics and metabolomics – advances in breast cancer profiling, *BMC Cancer* 2010, *10*, 128.
(20) Moestue, S. A.; Borgan, E.; Huuse, E. M.; Lindholm, E. M.; Sitter, B.; Børresen-Dale, A. L.; Engebraaten, O.; Mælandsmo, G. M.; Gribbestad, I. S., Distinct choline metabolic profiles are associated with differences in gene expression for basal-like and luminal-like breast cancer xenograft models, *BMC Cancer* 2010, *10*, 433.
(21) Sitter, B.; Bathen, T. F.; Singstad, T. E.; Fjøsne, H. E.; Lundgren, S.; Halgunset, J.; Gribbestad, I. S., Quantification of metabolites in breast cancer patients with different clinical prognosis using HR MAS MR spectroscopy, *NMR Biomed.* 2010, *23*, 424.
(22) Swanson, M. G.; Vigneron, D. B.; Males, R. G.; Kurhanewicz, J.; Tabatabai, Z. L.; Schmitt, L.; Carroll, P. R.; James, J. K.; Hurd, R. E.; Swanson, M. G., Proton HR-MAS spectroscopy and quantitative pathologic analysis of MRI/3D-MRSI-targeted postsurgical prostate tissues, *Magn. Reson. Med.* 2003, *50*, 944.
(23) Cheng, L. L.; Wu, C.-L.; Smith, M. R.; Gonzalez, R. G., Non-destructive quantitation of spermine in human prostate tissue samples using HRMAS 1H NMR spectroscopy at 9.4 T, *FEBS Lett.* 2001, *494*, 112.
(24) Swindle, P.; Ramadan, S.; Stanwell, P.; McCredie, S.; Russell, P.; Mountford, C., Proton magnetic resonance spectroscopy of the central, transition and peripheral zones of the prostate: assignments and correlation with histopathology, *Magn. Reson. Mater. Phys., Biol. Med.* 2008, *21*, 423.
(25) Van Asten, J. J. A.; Cuijpers, V.; Hulsbergen-Van De Kaa, C.; Soede-Huijbregts, C.; Witjes, J. A.; Verhofstad, A.; Heerschap, A., High resolution magic angle spinning NMR spectroscopy for metabolic assessment of cancer presence and Gleason score in human prostate needle biopsies, *Magn. Reson. Mater. Phys., Biol. Med.* 2008, *21*, 435.
(26) Moka, D.; Vorreuter, R.; Schicha, H.; Spraul, M.; Humpfer, E.; Lipinsky, M.; Foxall, P. J. D.; Nicholson, J. K.; Lindon, J. C., Magic angle spinning proton

nuclear magnetic resonance spectroscopic analysis of intact kidney tissue samples, *Anal. Commun*. 1997, *34*, 107.
(27) Tate, A. R.; Foxall, P. J. D.; Holmes, E.; Moka, D.; Spraul, M.; Nicholson, J. K.; Lindon, J. C., Distinction between normal and renal cell carcinoma kidney cortical biopsy samples using pattern recognition of ^{1}H magic angle spinning (MAS) NMR spectra, *NMR Biomed.* 2000, *13*, 64.
(28) Imperiale, A.; Elbayed, K.; Moussallieh, F. M.; Neuville, A.; Piotto, M.; Bellocq, J. P.; Lutz, P.; Namer, I. J., Metabolomic pattern of childhood neuroblastoma obtained by ^{1}H-high-resolution magic angle spinning (HRMAS) NMR spectroscopy, *Pediatr. Blood & Cancer* 2011, *56*, 24.
(29) Mountford, C. E.; Delikatny, E. J.; Dyne, M.; Holmes, K. T.; Mackinnon, W. B.; Ford, R.; Hunter, J. C.; Truskett, I. D.; Russell, P., Uterine cervical punch biopsy specimens can be analyzed by ^{1}H MRS, *Magn. Reson. Med.* 1990, *13*, 324.
(30) Mahon, M. M.; Cox, I. J.; Dina, R.; Soutter, W. P.; McIndoe, G. A.; Williams, A. D.; DeSouza, N. M., ^{1}H magnetic resonance spectroscopy of preinvasive and invasive cervical cancer: in vivo-ex vivo profiles and effect of tumor load, *J. Magn. Reson. Imaging* 2004, *19*, 356.
(31) Dave, U.; Taylor-Robinson, S. D.; Walker, M. M.; Mahon, M.; Puri, B. K.; Thursz, M. R.; Desouza, N. M.; Cox, I. J., In vitro ^{1}H-magnetic resonance spectroscopy of Barrett's esophageal mucosa using magic angle spinning techniques, *Eur. J. Gastroenterol. Hepatol.* 2004, *16*, 1199.
(32) Piotto, M.; Moussallieh, F. M.; Dillmann, B.; Imperiale, A.; Neuville, A.; Brigand, C.; Bellocq, J. P.; Elbayed, K.; Namer, I. J., Metabolic characterization of primary human colorectal cancers using high resolution magic angle spinning 1H magnetic resonance spectroscopy, *Metabolomics* 2009, *5*, 292.
(33) Chan, E. C. Y.; Koh, P. K.; Mal, M.; Cheah, P. Y.; Eu, K. W.; Backshall, A.; Cavill, R.; Nicholson, J. K.; Keun, H. C., Metabolic profiling of human colorectal cancer using high-resolution magic angle spinning nuclear magnetic resonance (HR-MAS NMR) spectroscopy and gas chromatography mass spectrometry (GC/MS), *J. Proteome Res.* 2009, *8*, 352.
(34) Seierstad, T.; Røe, K.; Sitter, B.; Halgunset, J.; Flatmark, K.; Ree, A. H.; Olsen, D.; Gribbestad, I. S.; Bathen, T. F., Principal component analysis for the comparison of metabolic profiles from human rectal cancer biopsies and colorectal xenografts using high-resolution magic angle spinning 1H magnetic resonance spectroscopy, *Mol. Cancer* 2008, *7*, 33.
(35) Lindon, J. C.; Beckonert, O. P.; Holmes, E.; Nicholson, J. K., High-resolution magic angle spinning NMR spectroscopy: application to biomedical studies, *Prog. Nucl. Magn. Reson. Spectrosc.* 2009, *55*, 79.
(36) Bathen, T. F.; Sitter, B.; Sjobakk, T. E.; Tessem, M.-B.; Gribbestad, I. S., Magnetic resonance metabolomics of intact tissue: a biotechnological tool in cancer diagnostics and treatment evaluation, *Cancer Res.* 2010, *70*, 6692.
(37) DeFeo, E. M.; Cheng, L. L., Characterizing human cancer metabolomics with ex vivo ^{1}H HRMAS MRS, *Technology in Cancer Research and Treatment* 2010, *9*, 381.
(38) Beckonert, O.; Keun, H. C.; Ebbels, T. M.; Bundy, J.; Holmes, E.; Lindon, J. C.; Nicholson, J. K., Metabolic profiling, metabolomic and metabonomic procedures for NMR spectroscopy of urine, plasma, serum and tissue extracts, *Nature Protocols* 2007, *2*, 2692.
(39) Lindon, J. C.; Nicholson, J. K.; Holmes, E.; Keun, H. C.; Craig, A.; Pearce, J. T. M.; Bruce, S. J.; Hardy, N.; Sansone, S. A.; Antti, H.; Jonsson, P.; Daykin, C.; Navarange, M.; Beger, R. D.; Verheij, E. R.; Amberg, A.; Baunsgaard, D.; Cantor, G. H.; Lehman-McKeeman, L.; Earll, M.; Wold, S.; Johansson, E.; Haselden, J. N.; Kramer, K.; Thomas, C.; Lindberg, J.; Schuppe-Koistinen, I.; Wilson, I. D.; Reily, M. D.; Robertson, D. G.; Senn, H.; Krotzky, A.; Kochhar,

S.; Powell, J.; Van Der Ouderaa, F.; Plumb, R.; Schaefer, H.; Spraul, M., Summary recommendations for standardization and reporting of metabolic analyses, *Nat. Biotechnol.* 2005, *23*, 833.
(40) Beckonert, O.; Coen, M.; Keun, H. C.; Wang, Y.; Ebbels, T. M.; Holmes, E.; Lindon, J. C.; Nicholson, J. K., High-resolution magic-angle-spinning NMR spectroscopy for metabolic profiling of intact tissues, *Nature Protocols* 2010, *5*, 1019.
(41) Carr, H. Y.; Purcell, E. M., Effects of diffusion on free precession in nuclear magnetic resonance experiments, *Phys. Rev*. 1954, *94*, 630.
(42) Louis, D. N.; Ohgaki, H.; Wiestler, O. D.; Cavenee, W. K.; Burger, P. C.; Jouvet, A.; Scheithauer, B. W.; Kleihues, P., The 2007 WHO classification of tumours of the central nervous system, *Acta Neuropathol.* 2007, *114*, 97.
(43) D'Adamo, Jr., A. F.; Peisach, J.; Manner, G.; Weiler, C. T., N acetyl aspartate amidohydrolase: purification and properties, *J. Neurochem.* 1977, *28*, 739.
(44) D'Adamo, Jr., A. F.; Smith, J. C.; Woiler, C., The occurrence of N-acetylaspartate amidohydrolase (aminoacylase II) in the developing rat, *J. Neurochem.* 1973, *20*, 1275.
(45) Opstad, K. S.; Bell, B. A.; Griffiths, J. R.; Howe, F. A., An assessment of the effects of sample ischaemia and spinning time on the metabolic profile of brain tumour biopsy specimens as determined by high-resolution magic angle spinning (1)H NMR, *NMR Biomed.* 2008, *21*, 1138.
(46) Jordan, K. W.; He, W.; Halpern, E. F.; Wu, C.-L.; Cheng, L. L., Evaluation of tissue metabolites with high resolution magic angle spinning MR spectroscopy human prostate samples after three-year storage at –80°C, *Biomark. Insights* 2007, *2*, 147.
(47) Waters, N. J.; Garrod, S.; Farrant, R. D.; Haselden, J. N.; Connor, S. C.; Connelly, J.; Lindon, J. C.; Holmes, E.; Nicholson, J. K., High-resolution magic angle spinning 1H NMR spectroscopy of intact liver and kidney: optimization of sample preparation procedures and biochemical stability of tissue during spectral acquisition, *Anal. Biochem.* 2000, *282*, 16.
(48) Wu, C. L.; Taylor, J. L.; He, W.; Zepeda, A. G.; Halpern, E. F.; Bielecki, A.; Gonzalez, R. G.; Cheng, L. L., Proton high-resolution magic angle spinning NMR analysis of fresh and previously frozen tissue of human prostate, *Magn. Reson. Med.* 2003, *50*, 1307.
(49) Middleton, D. A.; Bradley, D. P.; Connor, S. C.; Mullins, P. G.; Reid, D. G., The effect of sample freezing on proton magic-angle spinning NMR spectra of biological tissue, *Magn. Reson. Med.* 1998, *40*, 166.
(50) Sitter, B.; Bathen, T. F.; Tessem, M. B.; Gribbestad, I. S., High-resolution magic angle spinning (HR MAS) MR spectroscopy in metabolic characterization of human cancer, *Prog. Nucl. Magn. Reson. Spectrosc.* 2009, *54*, 239.
(51) Piotto, M.; Elbayed, K.; Wieruszeski, J. M.; Lippens, G., Practical aspects of shimming a high resolution magic angle spinning probe, *J. Magn. Reson.* 2005, *173*, 84.
(52) Findeisen, M.; Brand, T.; Berger, S., A ^{1}H-NMR thermometer suitable for cryoprobes, *Magn. Reson. Chem.* 2007, *45*, 175.
(53) Sukumar, S.; Johnson, M. O. N.; Hurd, R. E.; Zijl, P. C., Automated shimming for deuterated solvents using field profiling, *J. Magn. Reson*. 1997, *125*, 159.
(54) Van Zijl, P. C. M.; Sukumar, S.; Johnson, M. O. N.; Webb, P.; Hurd, R.E., Optimized shimming for high-resolution NMR using three-dimensional image-based field mapping, *J. Magn. Reson*. 1994, *111*, 203.
(55) Weiger, M.; Speck, T.; Fey, M., Gradient shimming with spectrum optimisation, *J. Magn. Reson.* 2006, *182*, 38.
(56) Elbayed, K.; Dillmann, B.; Raya, J.; Piotto, M.; Engelke, F., Field modulation effects induced by sample spinning: application to high-resolution magic angle spinning NMR, *Adv. Magn. Reson*. 2005, *174*, 2.

(57) Piotto, M.; Bourdonneau, M.; Furrer, J.; Bianco, A.; Raya, J.; Elbayed, K., Destruction of magnetization during TOCSY experiments performed under magic angle spinning: effect of radial B1 inhomogeneities, *J. Magn. Reson*. 2001, *149*, 114.
(58) Bathen, T. F.; Jensen, L. R.; Sitter, B.; Fjösne, H. E.; Halgunset, J.; Axelson, D. E.; Gribbestad, I. S.; Lundgren, S., MR-determined metabolic phenotype of breast cancer in prediction of lymphatic spread, grade, and hormone status, *Breast Cancer Res. Treat.* 2007, *104*, 181.
(59) Hong, Y. S.; Coen, M.; Rhode, C. M.; Reily, M. D.; Robertson, D. G.; Holmes, E.; Lindon, J. C.; Nicholson, J. K., Chemical shift calibration of 1HMAS NMR liver tissue spectra exemplified using a study of glycine protection of galactosamine toxicity, *Magn. Reson. Chem.* 2009, *47*, S47.
(60) Wishart, D. S.; Tzur, D.; Knox, C.; Eisner, R.; Guo, A. C.; Young, N.; Cheng, D.; Jewell, K.; Arndt, D.; Sawhney, S.; Fung, C.; Nikolai, L.; Lewis, M.; Coutouly, M. A.; Forsythe, I.; Tang, P.; Shrivastava, S.; Jeroncic, K.; Stothard, P.; Amegbey, G.; Block, D.; Hau, D. D.; Wagner, J.; Miniaci, J.; Clements, M.; Gebremedhin, M.; Guo, N.; Zhang, Y.; Duggan, G. E.; MacInnis, G. D.; Weljie, A. M.; Dowlatabadi, R.; Bamforth, F.; Clive, D.; Greiner, R.; Li, L.; Marrie, T.; Sykes, B. D.; Vogel, H. J.; Querengesser, L., HMDB: the human metabolome database, *Nucleic Acids Res.* 2007, *35*, D521.
(61) Akoka, S.; Barantin, L.; Trierweiler, M., Concentration measurement by proton NMR using the ERETIC method, *Anal. Chem*. 1999, *71* (*13*), 2554.
(62) Wider, G.; Dreier, L., Measuring protein concentrations by NMR spectroscopy, *J. Am. Chem. Soc.* 2006, *128*, 2571.
(63) Martinez-Bisbal, M. C.; Monleon, D.; Assemat, O.; Piotto, M.; Piquer, J.; Llacer, J. L.; Celda, B., Determination of metabolite concentrations in human brain tumour biopsy samples using HR-MAS and ERETIC measurements, *NMR Biomed*. 2009, *22*, 199.
(64) Provencher, S. W., Estimation of metabolite concentrations from localized in vivo proton NMR spectra, *Magn. Reson. Med.* 1993, *30*, 672.
(65) Fauvelle, F.; Dorandeu, F.; Carpentier, P.; Foquin, A.; Rabeson, H.; Graveron-Demilly, D.; Arvers, P.; Testylier, G., Changes in mouse brain metabolism following a convulsive dose of soman: a proton HRMAS NMR study, *Toxicology* 2010, *267*, 99.
(66) Wold, S.; Esbensen, K.; Geladi, P., Chemometrics and intelligent laboratory systems, *Chemom. Intell. Lab. Syst.* 1987, *2*, 37.
(67) Ebbels, T. M. D.; Cavill, R., Bioinformatic methods in NMR-based metabolic profiling, *Prog. Nucl. Magn. Reson. Spectrosc.* 2009, *55*, 361.
(68) Wold, S.; Sjöström, M.; Eriksson, L., PLS-regression: a basic tool of chemometrics, *Chemom. Intell. Lab. Syst.* 2001, *58*, 109.
(69) Tenenhaus, M., *La Régression PLS: Théorie et Pratique., Editions Technip*, Paris, France, 1998.
(70) Westerhuis, J. A.; Hoefsloot, H. C. J.; Smit, S.; Vis, D. J.; Smilde, A. K.; Velzen, E. J. J.; Duijnhoven, J. P. M.; Dorsten, F. A., Assessment of PLS-DA cross validation, *Metabolomics* 2008, *4*, 81.
(71) Lindon, J. C.; Holmes, E.; Nicholson, J. K., Pattern recognition methods and applications in biomedical magnetic resonance, *Prog. Nucl. Magn. Reson. Spectrosc.* 2001, *39*, 1.
(72) Motzer, R. J.; Bander, N. H.; Nanus, D. M., Medical progress: renal-cell carcinoma, *N. Engl. J. Med.* 1996, *335*, 865.
(73) Vogelzang, N. J.; Stadler, W. M., Kidney cancer, *Lancet* 1998, *352*, 1691.
(74) Allan, J. P.; Amnon, Z.; Arie, S. B., The changing natural history of renal cell carcinoma, *J. Urol.* 2001, *166*, 1611.

(75) Cheng, L. L.; Wu, C. L.; Smith, M. R.; Gonzalez, R. G., Non-destructive quantitation of spermine in human prostate tissue samples using HRMAS 1H NMR spectroscopy at 9.4 T, *FEBS Lett.* 2001, *494*, 112.
(76) Tomlins, A. M.; Foxall, P. J. D.; Lindon, J. C.; Lynch, M. J.; Spraul, M.; Everett, J. R.; Nicholson, J. K., High resolution magic angle spinning 1H nuclear magnetic resonance analysis of intact prostatic hyperplastic and tumour tissues, *Anal. Commun.* 1998, *35*, 113.
(77) Cheng, L. L.; Chang, I. W.; Smith, B. L.; Gonzalez, R. G., Evaluating human breast ductal carcinomas with high-resolution magic-angle spinning proton magnetic resonance spectroscopy, *J. Magn. Reson.* 1998, *135*, 194.
(78) Barton, S. J.; Howe, F. A.; Tomlins, A. M.; Cudlip, S. A.; Nicholson, J. K.; Bell, B. A.; Griffiths, J. R., Comparison of in vivo 1H MRS of human brain tumours with 1H HR-MAS spectroscopy of intact biopsy samples in vitro, *Magn. Reson. Mater. Phys., Biol. Med.* 1999, *8*, 121.
(79) Jordan, K. W.; Nordenstam, J.; Lauwers, G. Y.; Rothenberger, D. A.; Alavi, K.; Garwood, M.; Cheng, L. L., Metabolomic characterization of human rectal adenocarcinoma with intact tissue magnetic resonance spectroscopy, *Dis. Colon Rectum* 2009, *52*, 520.
(80) Tessem, M. B.; Selnaes, K. M.; Sjursen, W.; Tranø, G.; Giskeødegård, G. F.; Bathen, T. F.; Gribbestad, I. S.; Hofsli, E., Discrimination of patients with microsatellite instability colon cancer using ^{1}H HR MAS MR spectroscopy and chemometric analysis, *J. Proteome Res.* 2010, *9*, 3664.
(81) Delikatny, E. J.; Russell, P.; Hunter, J. C.; Hancock, R.; Atkinson, K. H.; Van Haaften-Day, C.; Mountford, C. E., Proton MR and human cervical neoplasia: ex vivo spectroscopy allows distinction of invasive carcinoma of the cervix from carcinoma in situ and other preinvasive lesions, *Radiology* 1993, *188*, 791.
(82) Sitter, B.; Bathen, T.; Hagen, B.; Arentz, C.; Skjeldestad, F. E.; Gribbestad, I. S., Cervical cancer tissue characterized by high-resolution magic angle spinning MR spectroscopy, *Magn. Reson. Mater. Phys., Biol. Med.* 2004, *16*, 174.
(83) Piotto, M.; Moussallieh, F. M.; Neuville, A.; Bellocq, J. P.; Elbayed, K.; Namer, I. J., Towards real-time metabolic profiling of a biopsy specimen during a surgical operation by 1H high resolution magic angle spinning nuclear magnetic resonance: a case report. *J. Med. Case Rep.* 2012, *6*, 22.